SEGMENTATION OF CELLULAR STRUCTURES IN ACTIN TAGGED FLUORESCENCE CONFOCAL MICROSCOPY IMAGES

B.J. Matuszewski[1], M.F. Murphy[2], D.R. Burton[2],
T.E. Marchant[3], C.J. Moore[3], A. Histace[4], F. Precioso[4,5]

[1]Applied Digital Signal and Image Processing Research Centre, UCLan, Preston, UK.
[2]General Engineering Research Institute, Liverpool John Moores University, Liverpool, UK.
[3]North Western Medical Physics, The Christie NHS Foundation Trust, Manchester, UK.
[4]ETIS UMR CNRS 8051, [5]LIP6 UMR CNRC 7606,

ABSTRACT

The paper reports on a novel method for reconstruction of cellular features including cell nuclei and cellular boundaries from actin tagged fluorescence confocal microscopy images. Such reconstruction can provide spatial context for subsequent quantitative analysis of changes to actin organisation and cell morphology in both controlled and stressed cell cultures. The proposed method is fully automatic and is formulated within active contour multiphase level set framework. The derived level set evolution PDEs combine previously proposed curvature and advection flows with propagation flow defined by specially designed set of geodesic distance maps. Additionally the proposed PDEs include additional components to impose known inclusion/exclusion topological constraints between cellular structures. The paper gives an overview of the proposed methodology as well as reports on initial results obtained for monolayer of human prostate cells (PNT2) culture visualised using acting tagged fluorescence confocal microscopy.

Index Terms— cell segmentation, active contour, geodesic distance, confocal microscopy, topological constraints

1. INTRODUCTION

The segmentation of cellular structures is an essential task in cell imaging as it provides information about cell morphology. This in turn enables measurements which can be used in analysis of cell differentiation, lineage tree or can provide data to calculate a cell proliferation rate, to name a few. More specifically, the work presented in this paper has been carried out in a context of cell cytoskeleton organization analysis. The results of this research will facilitate a large scale investigation of effects ionising radiation insult has on cytoskeleton structure, which forms part of a research effort aiming at better understanding of cells bio-mechanical responses during cancer radiation therapy. The cytoskeleton and more specifically actin filaments are implicated in a number of cellular processes, including cell adhesion, locomotion, intercellular transport and general cell structural integrity. From this perspective the segmentation of the cellular structures provides spatial reference frame for analysis of cytoskeleton changes.

The segmentation of nuclei and cell boundaries from actin tagged fluorescence confocal microscopy images is very demanding due to a highly complex actin appearance, high level of noise and strong non homogeneity of the intensity and gradient information of such images. The problem is further compounded by the missing, in places, indicators of cellular structures as well as presence of spurious indications of cell boundaries due to actin stress fibers forming, in monolayer cultures, in the intercellular spaces.

To date there has been a rather limited number of methods reported in the literature addressing segmentation of cellular structures in fluorescence confocal microscopy images (FCMI). Whereas the most of the published techniques address the problem of nuclei segmentation [1-3], there are only a very few papers concerned with segmentation of cellular boundaries. Method proposed in [4] uses Riemannian metric defined on 2D image manifold to calculate Voronoi regions seeded at given nuclei position. Each such region represents subsequently segmented cell. The main problem with this method is lack of interaction mechanism between nuclei and cell boundary segmentation, leading to under or over estimations of cellular structures. In [5] authors proposed technique for cell segmentation in two-dimensional images with two-channels (actin and nucleus tagging). The method uses a multiphase level set combing the Chan-Vese and geodesic active contour (GAC) models together with repulsive force introduced to prevent segmented cells from overlapping. In [6] authors described a technique for three-dimensional cell segmentation from a single channel actin tagged FCMI. That method is based on a generalized version of the subjective surface technique [7] which is known to cope well with missing boundary information.

As the methods described in [5], [6] the proposed in this paper algorithm also uses the level set framework. For each cell there are two level sets responsible respectively for segmentation of the cell boundary and nucleus. An evolution of each of these level sets is governed by a different PDE. Whereas the level sets representing nuclei are evolving according to a modified Chan-Vese model, the level sets representing cell boundaries use curvature and advection flow components derived from the GAC model together with a propagation flow calculated from a set of geodesic distance maps. Additionally each of the level sets interacts with the level set representing its own nucleus boundary and level sets representing boundaries of the neighboring cells. This additional interaction is introduced to preserve inclusion/exclusion topological constraints between cell nucleus and membrane and membranes of adjacent cells respectively. In this way the proposed method extends on the constraint proposed in [5] as that only included exclusion constraint. Additionally introduction of the geodesic distance maps makes the proposed method robust with respect to the missing boundary information. Although the method described in [6] has a

similar characteristic in terms of robustness to missing boundary information it is believed that the proposed here method copes better with actin stress fibers present in some monolayer cell cultures.

The remaining of this paper is organized as follows: in section 2 the data used in the experiments is introduced; section 3 explains different stages of the proposed segmentation algorithm whereas in section 4, results of the initial experimental validation of the method are presented; finally conclusions are drawn in section 5.

2. FLUORESCENCE CONFOCAL MICROSCOPY IMAGES

The data used in this paper was obtained from human prostate cells (PNT2) which were grown to confluence on glass coverlsips at 37 °C/5% CO_2 in modified Eagles Medium (MEM) supplemented with 10% bovine calf serum, 1% non-essential amino acids and 2 mM L-glutamine containing penicillin (100IU/mL) and streptomycin (100µg/ml). Once confluent cells were fixed and the actin labelled with phalloidin-FITC according to the manufacturer's instructions (Invitrogen, UK). All imaging was carried out using a Zeiss LSM510 confocal microscope. Figure 1 shows an example of the acquired image stack of the monolayer PNT2 cell culture. The stack volume is defined on the $512\times512\times98$ grid of voxels each $0.21\mu m\times0.21\mu m\times0.11\mu m$ in size.

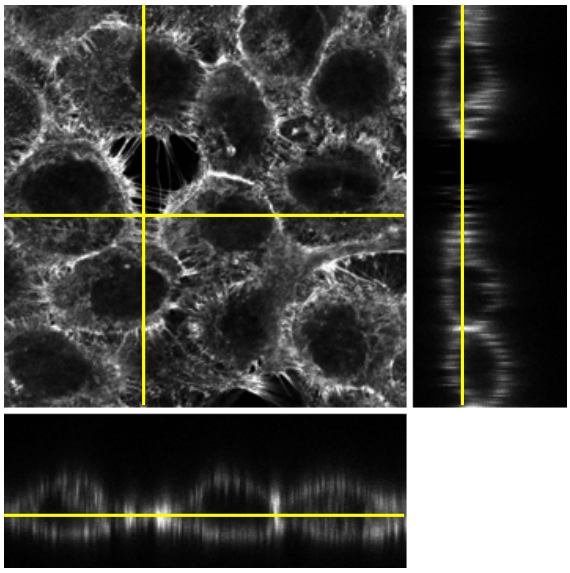

Fig. 1. Image stack showing monolayer of PNT2 cells. For the presentation purposes the data has been stretched along stack axis, by a factor of two to better visualise the structure of the data.

3. ALGORITHM

The proposed algorithm can be divided into two main processing stages. In the first preprocessing stage, which is data structure dependent, there are three steps: (i) estimation of the cellular background, (ii) selection of the central slide for algorithm initialization, and (iii) initial cell nuclei segmentation. In the second stage a specially designed multiphase level set active contours are simultaneously evolving to match cells' nuclei and boundaries. The level set evolutions are initialized based on initial nuclei segmentation results obtained in stage 1. The second stage is independent of the data structure and therefore it can be used with data representing multilayer cell cultures.

3.1. Image preprocessing

The preprocessing stage starts with the segmentation of the cell background seen in vertical and horizontal images shown in Figure 1 as predominantly black area above and below the cell monolayer. Although there are number of different ways to achieve that objective, the algorithm implemented here is based on the geodesic distance as defined by Eq. 3 and explained in the next section. The only difference introduced specifically for the cell background segmentation is that in this case "*R*" is given as a single point in the centre of the last image in the data stack. All voxels with the value of this distance bellow predefined threshold are treated as cells' background. The result of this operation, with the estimated cells background in white, is shown in Figure 2.

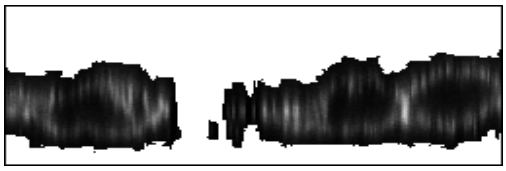

Fig. 2. Slice through the image stack volume after cell background segmentation. The position of the shown slice is indicated in figure 1 by vertical line.

The initial cell positions are estimated in the image selected as an equator slice through the monolayer, with the nuclei initial point positions, shown in Figure 3 as diamonds and pluses, estimated based on a simple thresholding. Both the slice and threshold selection is easily calculated from the 1D intensity profile obtained by accumulation of all the pixel intensities on each image slice. The detected points define a Voronoi diagram which in turn gives an estimated mapping for spatial cell occupancy, as shown in Figure 3. Only the cells for which Voronoi regions are completely included in the image are passed for further processing in the second stage.

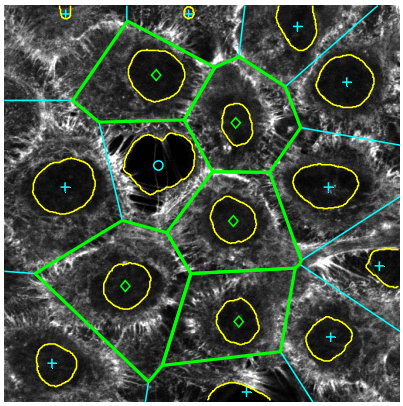

Fig. 3. Voronoi regions estimating initial cell positions, only regions marked by diamonds are further processed. Contours around centre of each Voronoi region show initial estimates of the cell nuclei.

In the last step of the preprocessing the nuclei are pre-segmented using Chan-Vese method, Eq. (8), with $\mu_{out(k)}$ $\mu_{in(k)}$ calculated within the corresponding Voronoi region as explained in the next section.

3.2. Multiphase level set segmentation

A generic form of the evolution equations used for segmentation of the cellular structures in the proposed method is given by [11],[12]:

$$\frac{\partial\phi(\mathbf{x},t)}{\partial t} = F(\mathbf{x},t)\,|\nabla\phi| + \lambda D(\mathbf{x};\mathbf{C}(t))\,|\nabla\phi| \qquad (1)$$

where: $\phi(\mathbf{x},t)$ represents evolving level set function with $\{\mathbf{x}:\phi(\mathbf{x},t)>0\}$ defining inside region of a given cellular structure; $F(\mathbf{x},t) = p(\mathbf{x},t) + \langle \vec{a}(\mathbf{x},t), \nabla\phi(\mathbf{x},t)/|\nabla\phi(\mathbf{x},t)| \rangle + c(\mathbf{x},t)\cdot\kappa$ is a velocity field with $p(\mathbf{x},t)$, $\vec{a}(\mathbf{x},t)$, $c(\mathbf{x},t)$ representing respectively propagation advection and curvature flows with curvature κ calculated as $\kappa=\mathrm{div}(\nabla\phi(\mathbf{x},t)/|\nabla\phi(\mathbf{x},t)|)$; $D(\mathbf{x};\mathbf{C}(t))$ denotes an additional velocity/force field introduced to preserve cells' topological configuration and λ is a weighting factor.

Eq. (1) has two different versions depending which cellular structure it is representing. Evolution equation for the level set representing k-th cell boundary, m(k), is derived from minimization of the following functional:

$$\begin{aligned} E(\phi_{\mathrm{m}(k)}(\mathbf{x})) &= \int_\Omega D_{f(k)}(\mathbf{x})\cdot H(\phi_{\mathrm{m}(k)}(\mathbf{x}))\,d\mathbf{x} \\ &+ \int_\Omega D_{b(k)}(\mathbf{x})\cdot(1-H(\phi_{\mathrm{m}(k)}(\mathbf{x})))\,d\mathbf{x} \\ &+ \alpha\int_\Omega g(\mathbf{x};I)\cdot|\nabla H(\phi_{\mathrm{m}(k)}(\mathbf{x}))|\,d\mathbf{x} \end{aligned} \qquad (2)$$

where: $\mathrm{D}_{f(k)}(\mathbf{x})$ and $\mathrm{D}_{b(k)}(\mathbf{x})$ are geodesic distance functions corresponding respectively to the foreground (inside) and background (outside) regions of the k-th cell. The foreground geodesic distance function is defined as:

$$D_{f(k)}(\mathbf{x}) = \inf_{S\in\mathcal{S}_{f(k)}} \int_0^1 G(S(p);I)\cdot|S'(p)|\,dp \qquad (3)$$

with $S(p)$ representing an open curve with parameterization p normalized in the range of [0,1], i.e., $S:[0,1]\rightarrow\mathbf{R}^3\in\Omega$ with Ω denoting the entire image domain and $\mathbf{x}$ denoting the coordinates of a point in that domain; $\mathcal{S}_{f(k)}$ represents a set of curves that connect the point $\mathbf{x}$ and the region R_k representing initially segmented k-th nucleus, i.e. $\mathcal{S}_{f(k)} = \{S : S(0) = \mathbf{x} \text{ and } S(1)\in R_k\}$. The geodesic metric is calculated using: $G(\mathbf{x};I) = |\mathbb{G}_\sigma * \nabla I(\mathbf{x})|$, where $\mathbb{G}_\sigma$ is Gaussian smoothing kernel.

Similarly the background geodesic distance function $\mathrm{D}_{b(k)}(\mathbf{x})$ for the k-th cell is given by:

$$D_{b(k)}(\mathbf{x}) = \inf_{S\in\mathcal{S}_{b(k)}} \int_0^1 G(S(p);I)\cdot|S'(p)|\,dp \qquad (4)$$

with $\mathcal{S}_{b(k)} = \{S : S(0) = \mathbf{x} \text{ and } S(1)\in\bigcup_{i\neq k} R_i\}$, where the union $\bigcup_{i\neq k} R_i$ is calculated over the image background region, detected in the first stage of the algorithm, and all initially detected cell nuclei expect the nucleus of the k-th cell.

Since the geodesic metric $G(\mathbf{x},I)$ is nonnegative, the geodesic distance functions can be calculated by solving the following eikonal equations:

$$\begin{cases} |\nabla D_a(\mathbf{x})| = G_a(\mathbf{x};I) \\ D_a(\mathbf{x}) = 0 \text{ for } \forall\ \mathbf{x}\in R_a \end{cases} \qquad (5)$$

where $a\in\{f(k),b(k)\}$. An Efficient approach to numerically solve this type of equations can be found in [9].

By deriving the Gateaux derivative of the proposed functional (2), the implicit PDE, describing the evolution process of the level set function to achieve function minimization, can be expressed as:

$$\begin{aligned} \frac{\partial\phi_{m(k)}(\mathbf{x},t)}{\partial t} &= (D_{b(k)}(\mathbf{x}) - D_{f(k)}(\mathbf{x}))\,|\nabla\phi_{m(k)}(\mathbf{x},t)| \\ &+ \alpha\,\mathrm{div}\left(g(\mathbf{x};I)\cdot\frac{\nabla\phi_{m(k)}(\mathbf{x},t)}{|\nabla\phi_{m(k)}(\mathbf{x},t)|}\right)|\nabla\phi_{m(k)}(\mathbf{x},t)| \end{aligned} \qquad (6)$$

The last term, weighted by a positive scalar α, is from the GAC model [10] used for accurate location of object boundary, wherein $g(\mathbf{x};I) = 1/(1+\beta G(\mathbf{x};I)^2)$ is the implemented edge indication function.

For practical reasons when selecting algorithm design parameters it is convenient for the propagation map to be normalised between -1 and 1. For this reason $(D_{b(k)}(\mathbf{x}) - D_{f(k)}(\mathbf{x}))$ propagation map in Eq (6) has been replaced with

$$p(\mathbf{x},t) = 2\cdot\mathrm{atan}\left(\gamma D_{b(k)}(\mathbf{x})/D_{f(k)}(\mathbf{x})\right)/\pi \qquad (7)$$

where γ controls "saturation point" of the propagation map.

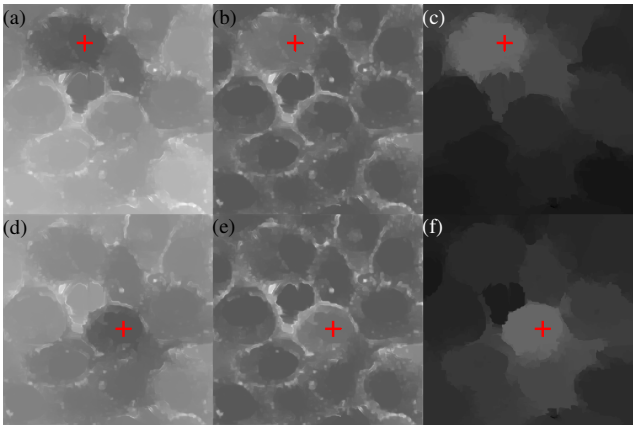

Fig. 4. Examples of the cells foreground and background geodesic distance maps $D_{f(k)}(\mathbf{x})$ {a,d}, $D_{b(k)}(\mathbf{x})$ {b,e} and corresponding propagation maps {c,f} as defined by Eq. (7) calculated for two different cells. Red crosses indicate initially estimated cell centers (see Figure 3).

The evolution equation for the k-th nuclei, n(k), segmentation is a version of the Chan-Vese method:

$$\frac{\partial\phi_{\mathrm{n}(k)}(\mathbf{x},t)}{\partial t} = \left((I-\mu_{out(k)})^2 - (I-\mu_{in(k)})^2 + \beta\kappa\right)|\nabla\phi_{\mathrm{n}(k)}| \qquad (8)$$

where mean values $\mu_{out(k)}$, $\mu_{in(k)}$ are calculated within region $\{\mathbf{x}:\phi_{m(k)}(\mathbf{x},t)>0\}$ representing evolving estimate of the k-th cell. As mentioned in section 3.1 the initial cell nuclei estimation uses the same model but with $\mu_{out(k)}$, $\mu_{in(k)}$ calculated within corresponding Voronoi region (see Figure 3).

The additional forces, $D_k(\mathbf{x};\mathbf{C}(t))$, in Eq (1) are defined as:

$$D_k(\mathbf{x};\mathbf{C}(t)) = -f(\mathrm{sdf}(\mathbf{x};M_k^{(i)})) + f(\mathrm{sdf}(\mathbf{x};M_k^{(o)})) \qquad (9)$$

These forces are used in both, nuclei and cell boundary level set evolutions. Their role is to prevent evolving active contours from intersecting and therefore enforcing inclusion (nucleus to reside inside the cell boundary) and exclusion (any two different cells should not occupy the same space) constraints. In the proposed algorithm $f(x) = sign(x)\exp(-x^2)$ what effectively means that these forces are activated only in the regions where contour is getting too close to its medial axis, $M_k^{(s)}$, as measured by the signed distance function, $\mathrm{sdf}(\mathbf{x}; M_k^{(s)})$, (index $s \in \{i, o\}$ indicates if the medial axis is located inside or outside of the *k*-th contour). The calculation of these forces introduces only a small computational overhead as calculation of the $\mathrm{sdf}(\mathbf{x}; M_k^{(s)})$, requires only addition and subtraction of active contours' signed distance functions which are already available. More information on how to calculate $M_k^{(s)}$ for simple level set configurations is given in [12].

4. EXPERIMENTAL RESULTS

The described algorithm has been tested on a small number of actin tagged fluorescence confocal microscopy image stacks. Figure 5 shows the results, obtained using 2D version of the algorithm, for two images selected from the stack shown in Figure 1. It can be noticed that the algorithm was able to extract cell boundaries despite of missing and "false" cell indicators. Although no truly quantitative assessment of the method has been undertaken so far, the results have been assessed qualitatively by a trained biologist who confirmed correctness of the detected structures. The algorithm has been tested in terms of its stability with respect to changes to its design parameters, and although there have been observed some variability of the segmentation results these were at the level typical for active contour methods.

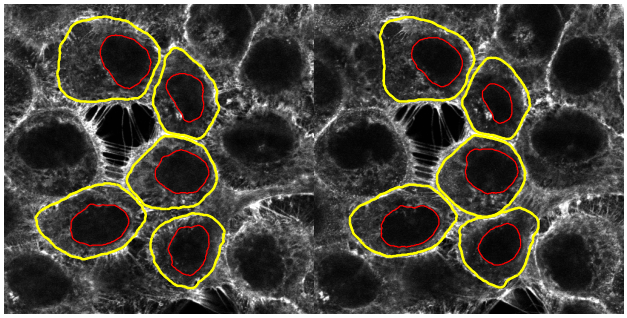

Fig. 5. Nucleus (in red) and cell boundaries (in yellow) segmented in stack of images from Figure 1, shown in two selected slices.

To quantitatively validate the proposed algorithm, many more tests with different image stacks representing different cell types will be conducted in a near future. For such analysis to have any practical meaning it is necessary though to build a comprehensive database of segmented cells, annotated by different experts to enable corrections for inter- and intra- observer variability, in the analysis of the accuracy of the method.

5. CONCLUSIONS

The paper describes a novel method for topologically consistent segmentation of cellular structures in the images obtained from the actin tagged fluorescence confocal microscopy images. The novelty of the method is in the proposed multiphase geodesic distance map region competition combined with the topology preserving medial axis constrained introduced to the level set evolution equations. The initial experimental results suggest that the method not only copes well with missing cell boundary information but also, contrary to previously proposed methods, is resilient to spurious structures formed by actin stress fibres in monolayer cell cultures. Although more comprehensive, quantitative validation of the method is needed before full conclusion could be drawn about its performance. It is believed that the method is suitable for large scale experiments aiming to develop a model of cytoskeleton response to ionising radiation insult.

6. REFERENCES

[1] C. Ortiz de Solorzano, E.G. Rodriguez, A. Jones, D. Pinkel, J.W. Gray, D. Sudar, and s.J. Lockett, "Segmentation of confocal microscope images of cell nuclei in thick tissue section," *J. Microsc.*, vol. 193, no. 3, pp.212-226, 1999.

[2] W. Wang, W. He, D. Metaxas, R. Mathew, and E. White, "Cell segmentation and tracking using texture-adaptive snakes," in *Proc. 4th IEEE Int. Sym. Biomedical Imaging: From Nano to Macro*, pp.101-104, 2007

[3] A. Sarti, C. Ortiz de Solarzano, S. Lockett, and R. Malladi, "A geometric model for 3-D confocal image analysis," *IEEE Trans. Biomed. Eng.*, vol. 47, pp. 1600-1609, 2000.

[4] T.R. Jones, A. Carpenter and P. Golland, "Voronoi-based segmentation of cell on image manifolds," *Computer Vision for Biomedical Image Applications*, LCNS 3765 pp. 535-543, 2005.

[5] P. Yan, X. Zhou, M. Shah, S.T.C. Wong, " Automatic Segmentation of High-Throughput RNAi Fluorescent Cellular Images," *IEEE Transactions on Information Technology in Biomedicine*, vol. 12, no. 1, pp.109-117, 2008.

[6] C. Zanella, M. Campana, B. Rizzi, C. Melani, G. Sanguinetti, P. Bourgine, K. Mikula, N. Peyriéras, and a. Sarti, "Cell Segmentation from 3-D Confocal Images of Early Zebrafish Embryogenesis," *IEEE Trans. On Image Processing*, vol. 19, no. 3, pp.770-781, 2010.

[7] A. Sarti, R. Malladi, and J.A. Sethian, "Subjective Surfaces: A Geometric Model for Boundary Completion," *International Journal of Computer Vision*, vol. 46, no. 3, pp.201-221, 2002.

[8] Y. Zhang, B.J. Matuszewski, A. Histace, F. Precioso, J. Kilgallon, C. Moore, "Boundary Delineation in Prostate Imaging using Active Contour Segmentation Method with Interactively Defined Object Regions," *LNCS 6367*, pp.131-142, 2010.

[9] M.S. Hassouna, A.A. Farag, "MultiStencil Fast Marching Methods: A Highly Accurate Solution to the Eikonal Equation on Cartesian Domains," *IEEE PAMI*, vol. 29, pp.1563-1574, 2007.

[10] V. Caselles, R. Kimmel and G. Sapiro, "Geodesic Active Contours," *IJCV*, vol. 22, pp. 61-79, 1997.

[11] Y. Zhang, B.J. Matuszewski, L.-K. Shark, C. Moore, "Medical Image Segmentation Using New Hybrid Level-Set Method", in MEDi08VIS, London, July 9-11, 2008.

[12] Y. Zhang, B.J. Matuszewski, "Multiphase Active Contour Segmentation Constrained by Evolving Medial Axes", in *Proceedings of IEEE ICIP'2009 Conference*, pp.2993-2996.

ACKNOWLEDGMENTS

This work was supported by the Engineering and Physical Science Research Council [grant number EP/H024913/1].